Int. Journ. of Unconventional Computing, Vol. 7, pp. 481–499
Reprints available directly from the publisher
Photocopying permitted by license only

Implementation of Microbe-Based Neurocomputing with *Euglena* Cells Confined in Micro-Aquariums

KAZUNARI OZASA[1], JEESOO LEE[2], SIMON SONG[2],
MASAHIKO HARA[1] AND MIZUO MAEDA[1]

[1]*RIKEN Advanced Science Institute, 2-1 Hirosawa, Wako, Saitama 351-0198, Japan*
[2]*Department of Mechanical Engineering, Hanyang University, 17 Haendang-dong, Seongdong-gu, Seoul, 133-791, Korea*
E-mail: ozasa@riken.jp

Received: January 14, 2011. Accepted: March 3, 2011.

Using real *Euglena* cells in a micro-aquarium as photoreactive biomaterials, we demonstrated *Euglena*-based neurocomputing with two-dimensional optical feedback using the modified Hopfield–Tank algorithm. The blue light intensity required to evoke the photophobic reactions of *Euglena* cells was experimentally determined, and the empirically derived auto-adjustment of parameters was incorporated in the algorithm. The *Euglena*-based neurocomputing of 4-city traveling salesman problem possessed two fundamental characteristics: (1) attaining one of the best solutions of the problem and (2) searching for a number of solutions via dynamic transition among the solutions (multi-solution search). The spontaneous reduction in cell number in illuminated areas and the existence of photo-insensitive robust cells are the essential mechanisms responsible for the two characteristics of the *Euglena*-based neurocomputing.

Keywords: Microbe-based neurocomputing, *euglena gracilis*, micro-aquarium, optical feedback, phototaxis, travel salesman problem (TSP), neural network, biocomputing, flagellate microbial cells, microchannels

1 INTRODUCTION

Living biomaterials, such as cells and microbes, generally show flexible strategies to survive against imposed stimuli and hence possess fascinating potential for information processing. Some microbes have sensors to detect

environmental stimuli and have flagellum to move toward more favorable conditions, i.e., taxis, such as phototaxis [1–4] and chemotaxis [5–9]. In other words, sensing (input), signal processing/transmission (computation), and actuating (output) are built in the body of the flagellate microbes as molecular level chemical reactions [10–13]. For instance, *Euglena gracilis* exhibits phototaxis reaction to external light: sensing the light intensity, determining the need to change the direction of swimming, and turning toward moderate light that is more favorable for photosynthesis [14,15]. Beyond this simple phototaxis reaction, more advanced/sophisticated reactions to the external stimuli can be observed: adaptation to the stimuli (learning), alternative reactions to survive (exploiting), the variation in reaction threshold (personality), or the memorization of stimuli history [16–18]. When these advanced/sophisticated reactions of the microbes are used in information processing, we can expect that the processing will be robust against noise or fluctuation, adaptive to unexpected rules or tasks, or advantageous to search new solutions.

Microbe-based information processing has been intensively investigated using unicellular amoeba (plasmodium of the true slime mould Physarum polycephalum) [19–29]. Nakagaki et al. demonstrated that a slime mould spontaneously forms shortest paths that connect detected foods using its food-searching and effective nutrition-transportation capability [19,25]. Aono et al. implemented the solution search of combinatorial optimization problems using a single slime mould in an optical feedback system with neural network algorithms [23,26,28]. In amoeba-based neurocomputing, food-searching capability and photophobic reaction of the slime mould were used for driving neurocomputation. Because a slime mould is a unicellular microbe, even when the body of the slime mould expands to a cm-wide space, the information on which part of the body is exposed to the external stimuli can be shared among the whole parts of the slime mould body, contributing to the cooperative behavior of the whole parts of the cm-wide slime mould.

By constructing a two-dimensional (2D) microscopic optical feedback system, similar neurocomputing may be realized with other phototaxis microbes of micrometer scales. We examined the possibility to use *Euglena* cells as photoreactive biomaterials for computing using the Monte Carlo simulation of neurocomputing [30,31]. The photophobic reactions of *Euglena* were experimentally obtained, simplified, and incorporated in the Monte Carlo simulation. The simulation of *Euglena*-based neurocomputing proved that it can solve the same traveling salesman problem (TSP) that Aono et al. solved by their amoeba-based neurocomputing [23,26,28]. The simulation also demonstrated two fundamental characteristics of microbe-based neurocomputing: (1) attaining one of the best solutions of the problem, and (2) searching for a number of solutions via dynamic transition among the solutions (multi-solution search). However, the study has revealed that the mechanisms behind these characteristics are different for amoeba-based and *Euglena*-based neuro-

computing: the cooperative food-search characteristics of a slime mould versus statistical fluctuation in *Euglena* movements [30,31].

In the Monte Carlo simulation of *Euglena*-based neurocomputing, we assumed that all the *Euglena* cells had the same photophobic characteristics that they swim in a straight path in the dark, and that their swimming speeds are reduced to one tenth of the original speeds by light irradiation. Real *Euglena* cells swim in a winding path and show variation in photosensitivity, i.e., some cells are insensitive and robust to light irradiation. These differences will influence the performance of *Euglena*-based neurocomputing. Moreover, real *Euglena* cells may exhibit various survival strategies against the external photo stimuli, such as changing photosensitivity, migrating in light, or swiftly turning on encountering light. Therefore, the characteristics and performance of *Euglena*-based neurocomputing must be verified with real *Euglena* cells.

In this report, we describe the implementation of neurocomputing with real *Euglena* cells confined in micro-aquariums. Two new techniques were introduced to achieve real-time *Euglena*-based neurocomputing: (1) we measured trace momentums (TMs) of specified areas instead of measuring the swimming speed of each cell to realize real-time optical feedback-stimulation to *Euglena* cells, (2) parameters in sigmoid function were adjusted in real time with empirically derived auto-adjustment equations. *Euglena*-based neurocomputing was realized with these two techniques and performance comparative to amoeba-based neurocomputing was achieved, although the mechanisms of the performance were completely different. The essential mechanisms of *Euglena*-based neurocomputing were discussed by analyzing the distribution of *Euglena* cells in the illuminated/non-illuminated areas and the existence of photo-insensitive robust cells.

2 EXPERIMENTAL

2.1 Euglena gracilis

Euglena gracilis is a common microbe living in pure water [32–34], which swims with its flagellum at a speed of 100–400 μm/s. The size of each *Euglena* cell is approximately 50–80 μm long and 10–30 μm in diameter. The swimming movements of *Euglena* cells largely depend on the environmental light intensity. Because they live either by heterotrophy or photosynthesis in moderate daylight, they change their swimming direction to stay in moderate light favorable for photosynthesis; when they encounter "harmfully strong" blue light, they turn to escape from the light [1,2,14]. This photophobic reaction of *Euglena* is evoked by blue light above approximately 10 mW/cm^2 [1,2,14]. When they fail to escape from the strong blue light and are captured in the light, they continuously turn in their position,

like a spinning top, and drift meanderingly. Cramer–Myers' medium [35] was used to culture the *Euglena* cells in this study.

2.2 Micro-aquariums

We prepared a micro-aquarium by using poly-dimethyl-siloxane (PDMS) moulding [Fig. 1(a)]. The micro-aquarium had 16 equivalent branches (184 μm in width), allocated around a center circle of 1.1-mm diameter, and the outer diameter of the pattern was 2.5 mm. The two-dimensional configuration of the micro-aquarium was the same as that we used in our Monte Carlo simulation. The micro-aquarium depth was approximately 100 μm suf-

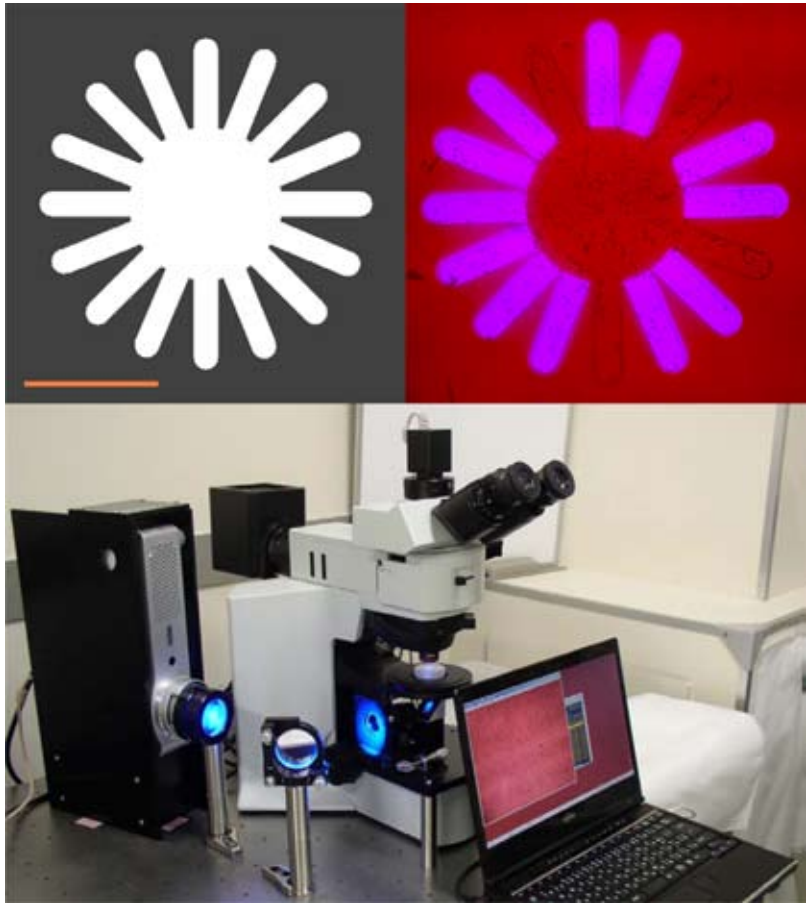

FIGURE 1
(a, top left) Micro-aquarium pattern with 16 equivalent branches in which *Euglena* cells were confined for neurocomputing. (b, top right) An example of a raw image of the micro-aquarium with *Euglena* cells where 12 branches were illuminated by blue light. (c, bottom) A picture of our 2D microscopic optical feedback system for *Euglena*-based neurocomputing.

ficiently large to allow *Euglena* cells to swim across each other without collisions. The total volume of the micro-aquarium was approximately 0.30 mm^3 and each branch occupied 0.012 mm^3.

A 10-μl droplet of water containing *Euglena* cells (100–1000 cells/mm^3) was placed on the PDMS micro-aquarium. The micro-aquarium was then covered with a 25-mm-diameter cover glass, sealed in a 30-mm-diameter glass-bottomed dish, and placed on the stage of an optical microscope (BX51, Olympus).

2.3 Two-dimensional feedback system

The 2D optical feedback system we developed [30,31,36] is shown in Fig. 1(c). The system was constructed with the optical microscope on which the *Euglena* dish was placed, an image capturing system with a 5X objective lens (MPLFLN5X, Olympus), a video camera (IUC-200CK2, Trinity), image processing personal computer (PC, MG/D70N, Fujitsu), a liquid crystal (LC) projector (LP-XU84, Sanyo) to irradiate 2D optical feedback patterns on the *Euglena* dish, and a lens/mirror system to reduce the scale of the optical projection pattern. The system had a resolution of 200 pixel/mm in both image capturing and pattern projection. Light onto one branch did not affect neighbouring *Euglena* cells in non-illuminated branches, because the spatial resolution and the contrast of the illumination were sufficiently high [Fig. 1(b)] to induce the photophobic reactions of *Euglena* cells only in the illuminated branches.

The raw images of *Euglena* cells in the micro-aquarium were captured at every 260-ms interval. An example of the raw images is given in Fig. 1(b). The movements of *Euglena* cells were extracted by subtracting the raw images frame-by-frame and binarizing the subtracted images by thresholding. Subsequently, 10 binary images were superimposed resulting in a *trace image*. Figure 2 shows the typical trace images of *Euglena* cells with and

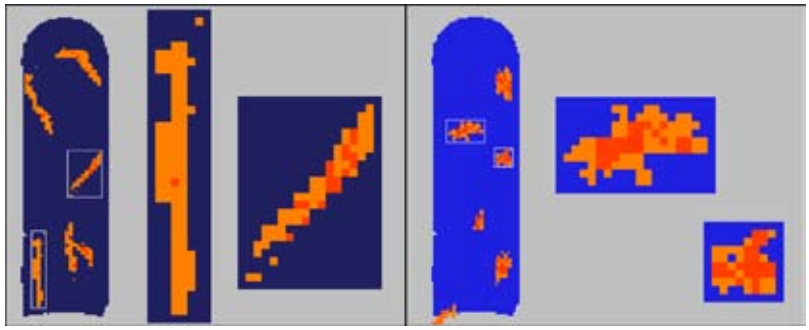

FIGURE 2
(a, left) Trace image obtained for a non-illuminated branch of micro-aquarium, with two magnified images. Dark orange pixels indicate the overlap of traces. (b, right) Trace image obtained for an illuminated branch of micro-aquarium with two magnified images.

without blue light irradiation. The swimming of a *Euglena* cell in a straight path without blue light yielded a straight line, whereas the rotational movement of the cell under blue light yielded a broadened spot. The trace images during the neurocomputing were stored in the PC memory and analyzed after the completion of neurocomputing.

2.4 Trace momentum and trace overlap momentum

The swimming speed of each *Euglena* can be measured in principle by a particle tracking velocimetry (PTV) technique [37,38]. However, PTV takes time to process the images and hence is not suitable for real time feedback operation. Instead of the sum of swimming speeds that we used as state variables in the Monte Carlo simulation, we designed two other types of indices as state variables: trace momentum (TM) and trace overlap momentum (TOM). TM is the number of ON pixels in a specified area (each entire branch in this study, although we can arbitrarily specify multiple measurement areas in the whole observation area) collected for 10 binary images. TOM is the number of ON pixels overlapped with the previous ON pixels in the superimposition of 10 binary images for a specified area. TM approximates the scalar summation of the swimming speeds of *Euglena* cells in the area, while TOM represents the scalar summation of the rotational movements of the cells in the area. TM becomes large when the area is not illuminated and many cells are swimming there, whereas TOM becomes large when the area is illuminated by blue light and many cells are turning continuously. TM and TOM for Fig. 2(a) are 607 and 77, respectively, whereas TM and TOM for Fig. 2(b) are 568 and 263, respectively.

To deduce the optimum blue light intensity, we evaluated the photosensitivity of *Euglena* cells by measuring TOM for the whole area of the micro-aquarium. In neurocomputing, we measured the TMs of 16 branches of the micro-aquarium.

2.5 Neurocomputing algorithm

We used the same algorithm and 4-city TSP as that examined in the Monte Carlo simulation of *Euglena*-based neurocomputing [30,31], employing the modified Hopfield–Tank model [39,40] with a fixed weight matrix w_{ij}, time step Δt, sigmoid function $\sigma(x)$, step function $f(x)$, and parameters b and c.

$$y_i(t+\Delta t) = f(\textstyle\sum_j^N w_{ij}\sigma(x_j(t))), \tag{1}$$

$$\sigma(x) = 1/(1+\exp(-b(x-c))), \tag{2}$$

$$\mathrm{f(x)} = 1 \quad \text{when } x > 1.0, \tag{3}$$

$$0 \quad \text{otherwise.}$$

$$w_{ij} = \begin{cases} \text{distance}/20 & \text{(between choices } i \text{ and } j\text{)}, \\ 1 & \text{(between invalid choices } i \text{ and } j\text{)}, \\ 0 & \text{(otherwise)}. \end{cases} \tag{4}$$

The 16 TMs measured for 16 branches of the micro-aquarium were used as the 16 state variables x_j ($j = 1..16$). When the feedback signal y_i ($i = 1..16$) was 1, the blue light of fixed intensity was irradiated on the corresponding branch i. Figure 3 shows the data processing chart. The repetition rate of the feedback was approximately 0.4 Hz, equal to the frequency of TM measurement, i.e., once per one cycle of the computing process shown in Fig. 3. One TM value was obtained with 10 raw-image capture, which requires approximately 2.6 s. The interval of raw image capture (260 ms) was selected to be close to (*Euglena* length)/(*Euglena* swimming speed).

The illustration of 4-city TSP with distance figures is shown in Fig. 4 with the eight best solutions for it. The 4-city TSP is mapped as the selection of branches, i.e., each branch was labeled with a city index (A, B, C, or D) and visiting order (1, 2, 3, or 4), as shown in Fig. 4. A set of non-illuminated branches ($y_i = 0$) correspond to a route; (A3, B4, C1, D2) corresponds to a route from C to D to A to B and back to C (total distance = 12). The valid solutions for the 4-city TSP are categorized into three: the eight best with

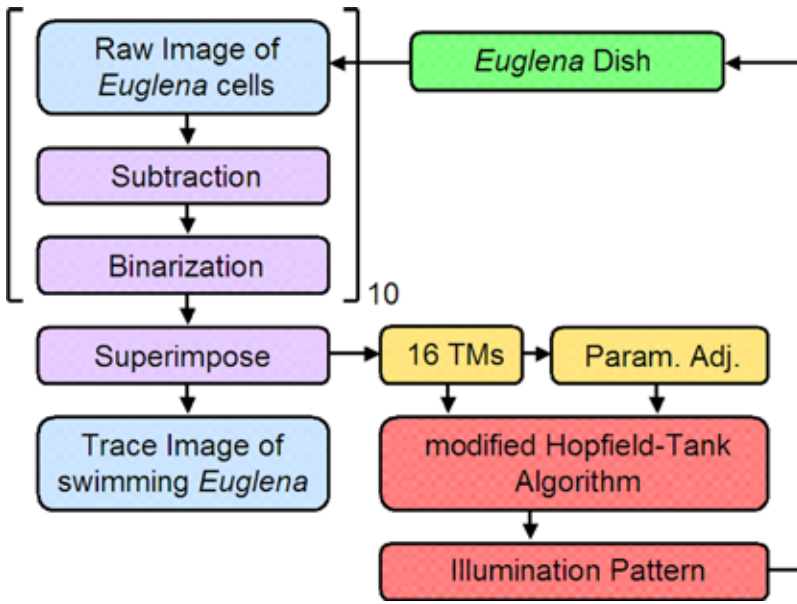

FIGURE 3
Data processing chart for *Euglena*-based neurocomputing.

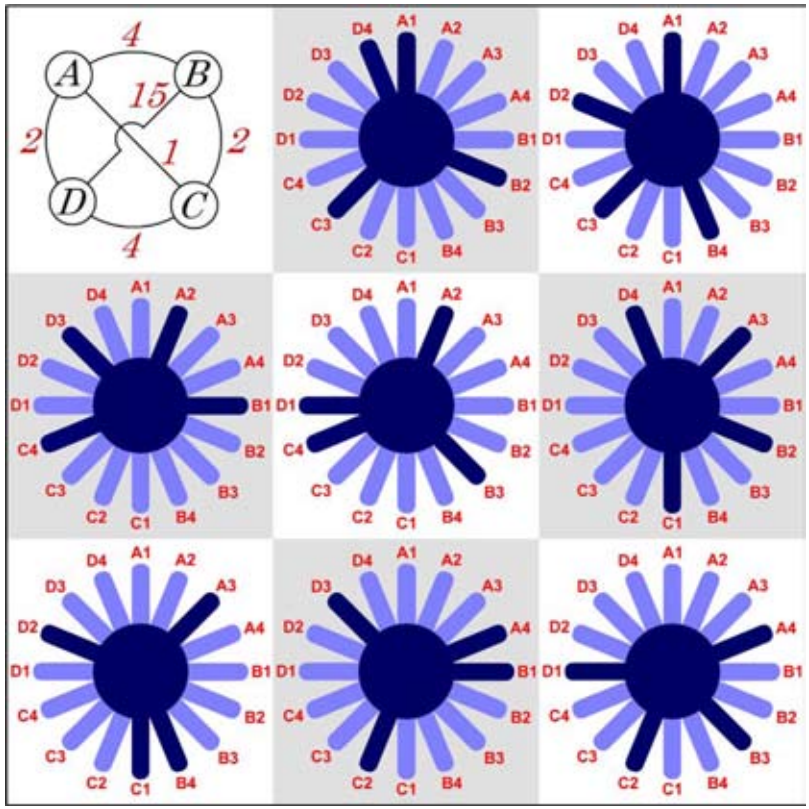

FIGURE 4
Illustration of 4-city traveling salesman problem with distance figures (top, left) and eight best solutions for the 4-city TSP. A set of non-illuminated branches represents the solution of city visiting order.

distance 12, the eight second best with distance 20, and the eight third best with distance 24. Although the solution (A3, B4, C1, D2) means the same route as (A1, B2, C3, D4), i.e., the route of A to B to C to D and back to A, we treated these equivalent solutions as individual ones.

3 RESULTS AND DISCUSSION

3.1 Optimization of blue light intensity

Figure 5 shows the temporal change in TOM observed for the whole area of the micro-aquarium, with alternatively switching blue light On and Off. The On- and Off-periods were 1.28 min each. The blue light intensity for On period was increased stepwise from 0.0 to 60 mW/cm^2. In this experiment, the whole area of the micro-aquarium was irradiated by blue light.

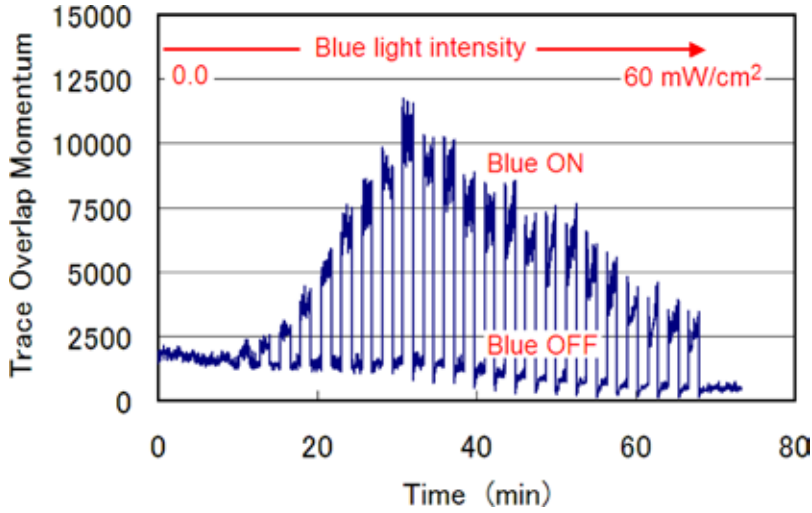

FIGURE 5
Temporal change in TOM measured for the whole area of the micro-aquarium by alternatively switching blue light On and Off. The blue light intensity for On period was increased stepwise from 0.0 to 60 mW/cm^2.

The photophobic reaction of *Euglena*, i.e., increase in TOM, was observed for blue light intensities above 1.1 mW/cm^2 (at 11 min), and it reached its maximum at 13.7 mW/cm^2 (at 31 min). Above 13.7 mW/cm^2, TOM decreased monotonically to one fourth of its maximum. Because TOM was the number of overlapped ON pixels in the subtracted and binarized image, the decrease in TOM for blue light intensity above 13.7 mW/cm^2 suggests that the *Euglena* cells tended to stay still rather than turn in position. TOM at Off period remained at the same level below 21.8 mW/cm^2 (at 39 min), whereas it decreased gradually above 24.9 mW/cm^2 (at 42 min). The decrease in TOM at Off period indicates that the blue light damaged the swimming capacity of the *Euglena* cells unrecoverably. Form these results, we used a blue light intensity of 18.8 mW/cm^2 in the neurocomputing experiments, which has enough margins to evoke photophobic reactions and not to induce damages in swimming capacity of *Euglena* cells.

3.2 Parameter auto-adjustment

Unlike the Monte Carlo simulation, the number of *Euglena* cells in the micro-aquarium cannot be controlled precisely resulting in non-reproducible average TMs in neurocomputing experiments. Furthermore, the photoinduced reduction of TM, which was defined as photoreaction ratio $\gamma =$ (TM with blue light)/(TM without blue light), fluctuates during the experiments. To perform *Euglena*-based neurocomputing with high performance, the uncertainties of TM and γ should be cancelled by adjusting the parameters b and c in Eq. (2).

Figure 6(a) shows the parameter dependence of neurocomputing performance calculated with the Monte Carlo simulation assuming that TM without blue light has a Gaussian probability distribution with an average of 22.0 with a standard deviation of 5.0 and photoreaction ratio $\gamma = 0.20$. The neurocomputing performance was evaluated by the number of time steps of the simulation that was occupied by the eight best solutions, i.e., (time steps at the best eight solutions)/(total time steps). The contours in parameter mapping for b and c in Fig. 6(a) show band structures. The small structures in Fig. 6 have little importance because they depend on the random num-

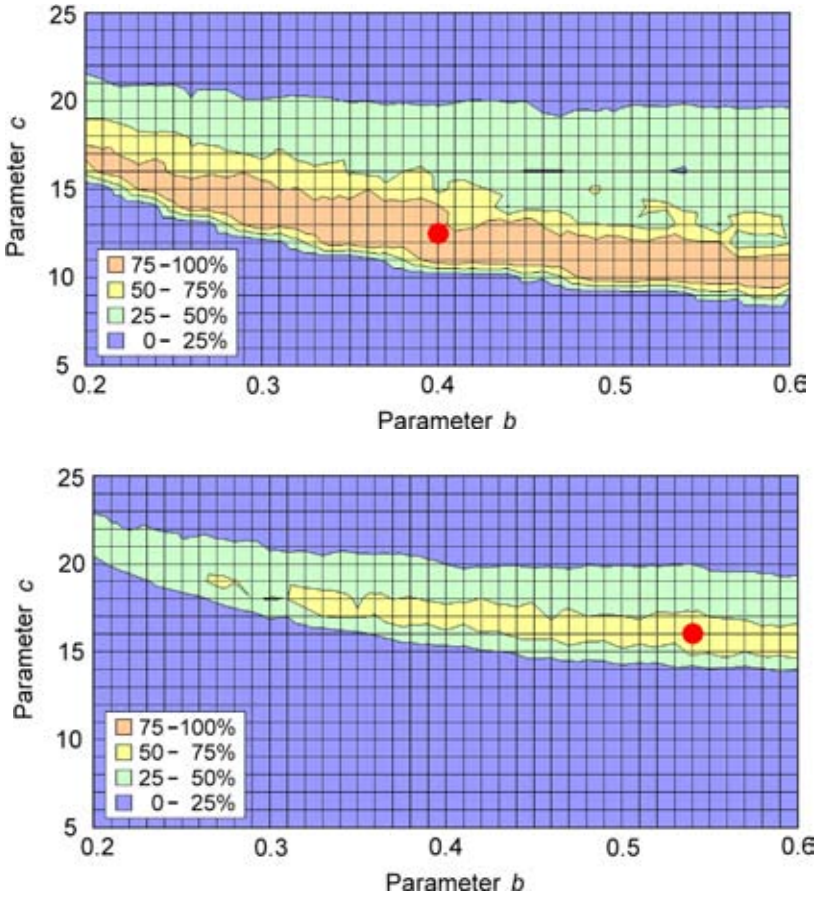

FIGURE 6

Parameter dependence of neurocomputing performance calculated with the Monte Carlo simulation assuming that TM without blue light has a Gaussian probability distribution with an average of 22.0 and a standard deviation of 5.0. Photoreaction ratio $\gamma = 0.20$ for (a, top) and 0.40 for (b, bottom). The performance was evaluated by occupation rate that is defined as the percentage of time steps occupied by the eight best solutions. Red points indicate the selected set of (b, c) for each γ.

bers used in the Monte Carlo simulation. We selected one best parameter set $(b,\ c) = (0.40,\ 12.5)$ for $\gamma = 0.20$. When the photoreaction ratio γ increases the neurocomputing performance decreases, as shown in Fig. 6(b) for $\gamma = 0.40$, revealing that the large photophobic reaction of *Euglena* is essential in *Euglena*-based neurocomputing. With a similar process for different γ, we obtained other best parameter sets $(b,\ c) = (0.31,\ 12.0)$ for $\gamma = 0.10$, $(0.46,\ 14.0)$ for $\gamma = 0.30$, $(0.54,\ 16.0)$ for $\gamma = 0.40$, and $(0.60,\ 18.5)$ for $\gamma = 0.50$.

The empirical equations $b(\gamma)$ and $c(\gamma)$ were deduced from these best parameter sets (Fig. 7), and expanded to arbitrary TM:

$$\gamma = \text{ave\_TM1/ave\_TM0}, \tag{5}$$

$$b(\gamma) = (0.72\gamma + \ 0.246) \times (22.0/\text{ave\_TM0}), \tag{6}$$

$$c(\gamma) = (32.1\gamma^2 - 2.79\gamma + 11.9) \times (\text{ave\_TM0}/22.0), \tag{7}$$

where ave_TM0 is the average of TM without blue light and ave_TM1 is that of TM with blue light. In the *Euglena*-based neurocomputing, the ave_TM0 and ave_TM1 were calculated from the 10 latest TMs with and without blue light, respectively. The parameters b and c were adjusted by Eqs. (5)–(7) every 10 cycles of feedback. Equations (5)–(7) give accurate adjustments when the temporal change of γ is moderate.

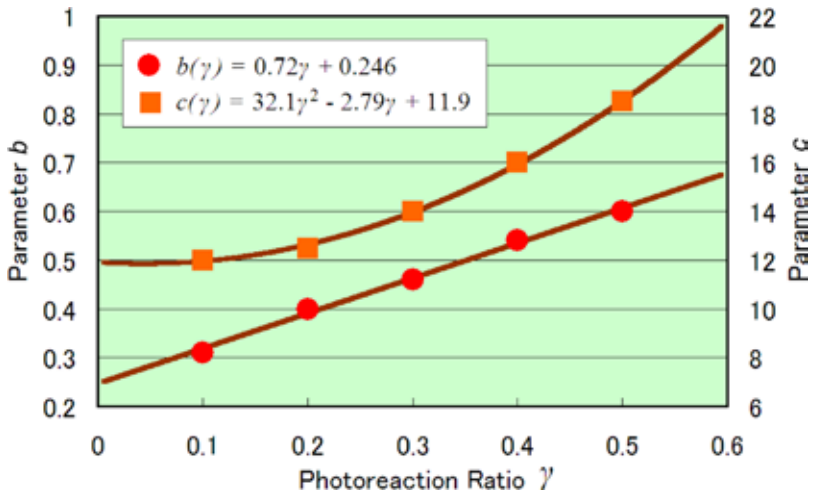

FIGURE 7
Dependence of $b(\gamma)$ and $c(\gamma)$ deduced from the selected parameter set $(b,\ c)$ for $\gamma = 0.1$, 0.2, 0.3, 0.4, and 0.5. The curves are fitting curves for $b(\gamma)$ with linear fitting and $c(\gamma)$ with parabolic fitting.

3.3 *Euglena*-based neurocomputing

Euglena-based neurocomputing was examined with the blue light intensity of 18.8 mW/cm^2, parameter auto-adjustment with Eqs. (5)–(7), and approximately 200 *Euglena* cells confined in the micro-aquarium. Figure 8(a) shows a typical example of state transitions during a single trial of the neu-

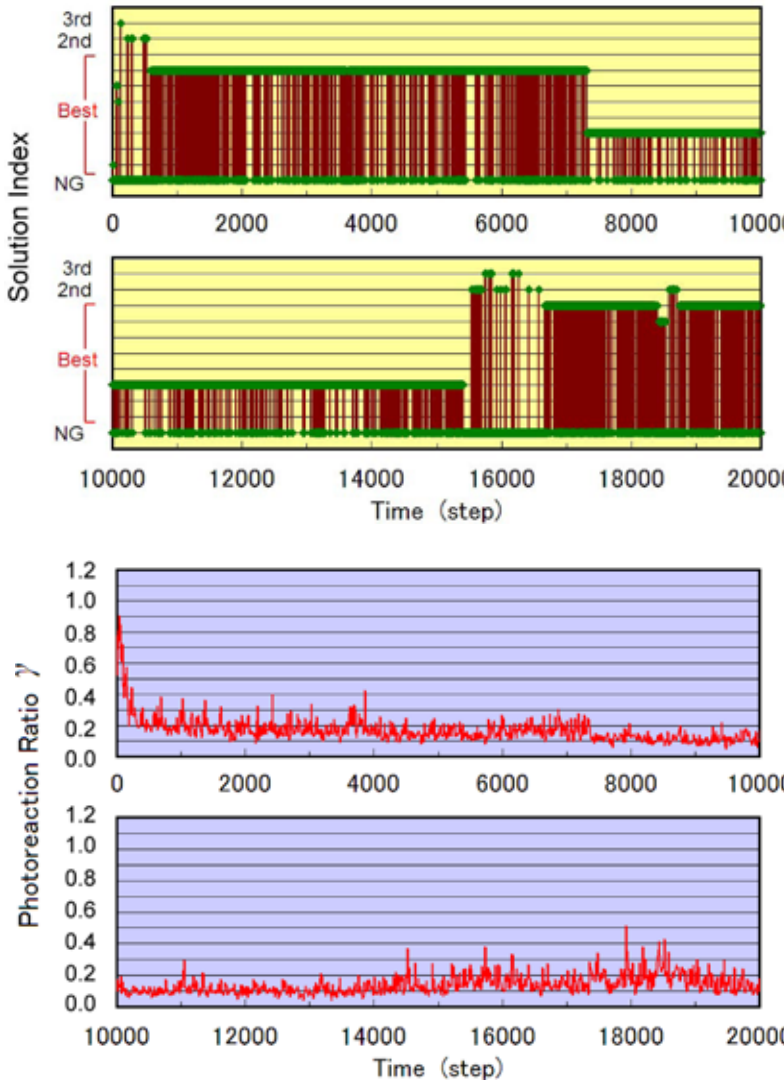

FIGURE 8

(a, top) Transition among the valid solutions observed in *Euglena*-based neurocomputing. The eight second and third best (worse) solutions are unified into two groups (2nd and 3rd), and invalid solutions are unified into one (NG). One time step corresponds to approximately 2.6 s. (b, bottom) Temporal change in the photoreaction ratio γ in the same experiment of (a).

rocomputing experiments. One time step in Fig 8(a) equals to approximately 2.6 s. After a short transition at the early stage of the experiment (0–610 time steps), the best solution #7 was achieved repeatedly for 611–7313 time steps. The best solution #7 occupied 85% of 600–7313 time steps. Invalid solutions appeared for 611-7313 time steps were mostly one-city missing (44% of invalid solution) or two-cities missing (43%) from the best solution #7. Another best solution #3 was achieved repeatedly for 7317–15410 time steps, resulting in the #3 occupation rate of 90% for this period. Invalid solutions appeared for 7317-15410 time steps were also one-city missing (44% of invalid solution) or two-city missing (37%) from the best solution #3. The system was then in transitional states until 16671 time step, and moved to another best solution #8 with the occupation rate of 64% for 16671–20000 time steps. The occupation rate of the best solutions in this trial was 77% in total. Two fundamental characteristics of *Euglena*-based neurocomputing, i.e., (1) attaining one of the best solutions of the problem and (2) searching for a number of solutions via dynamic transition among the solutions (multi-solution search), were experimentally verified in Fig. 8(a).

The transition among the solutions occurs primarily by the switching of two city orders: for instance, transition from #7 (A4, B1, C2, D3) to #3 (A2, B1, C4, D3) takes place by switching two components through invalid solutions of one- or two-city missing. The transition from #3 to #8 (A4, B3, C2, D1) observed in Fig. 8(a) for 15411–16670 time steps was bridged by intermediate solutions such as #12 (A2, B4, C3, D1) and #16 (A4, B2, C3, D1). The solution #12 and #16 were not the bests and did not remain longer. The invalid solutions of one- or two-city missing imply an increase in the TMs of illuminated branches. From the recorded trace images, we found that the increase was caused by photo-insensitive robust *Euglena* cells, which can continue swimming in the illuminated branches.

The temporal evolution of the photoreaction ratio γ is shown in Fig. 8(b). Although fluctuation was observed for all the periods of the experiment, γ decreased below 0.4 at the early stage of the experiment (before 240 time steps), and then remained mostly below 0.3. γ remained below 0.2 for 7360–14500 time steps, where the high occupation rate of 90% was obtained for the best solution #3. The average γ for the period of the best solutions #7, #3, and #8 was 0.17, 0.12, and 0.14, respectively. The average γ below 0.20 indicates that larger photophobic reactions of *Euglena* result in higher occupation rates for a certain best solution, i.e., the neurocomputing system stays at one of the best solutions for a longer period.

Euglena cells were spread in the micro-aquairum entirely at the beginning of the neurocomputing. Thus, the start condition differs from that of the amoeba-based neurocomputing or the Monte Carlo simulation, where a slime mould or cells were concentrated at the centre circle. However, we consider that the initial distribution of cells in the branches does not affect the neurocomputing

results, unless a large deviation in cell number exists across the branches. In the experiment in this report, the frequent change of illumination pattern was observed soon after *Euglena*-based neurocomputing started [Fig. 8(a)], showing that the initial deviation in cell number was not significant.

3.4 Comparison between real Euglena experiments and simulation

As we reported previously [30,31], the same characteristics (1) and (2) were obtained in the Monte Carlo simulation of neurocomputing with simplified photophobic reactions of *Euglena*. However, the mechanisms responsible for (1) and (2) differ considerably between the simulation and the real *Euglena* experiments. In the simulation, the photophobic reactions of *Euglena* cells were the one-tenth reduction in their swimming speeds, and therefore, the state variables were only the function of blue light irradiation and the spontaneous fluctuation. In other words, the photoreaction ratio γ in the simulation always remained approximately 0.1. On the other hand, the ratio γ in real *Euglena*-based neurocomputing showed a large reduction from 0.8 to 0.2 at the early stage of the experiment and then remained in the range of 0.2–0.4 thereafter [Fig. 8(b)].

TM approximates the scalar summation of the swimming speeds of *Euglena* cells in the area, and therefore is the function of the number of the *Euglena* cells in the specified area as well as the swimming speed of the cells. Figure 9 shows trace images taken at 650 (at the best solution #6) and 6440 time steps (at the best solution #7). The photoreaction ratio γ was 0.74 and 0.21 for Fig. 9(a) and 9(b), respectively. In Fig. 9(a), the average number of *Euglena* cells in one illuminated branch is close to that in one non-illuminated branch. Therefore, the photophobic movements of *Euglena* cells caused the γ of 0.74 for Fig. 9(a). On the other hand in Fig. 9(b), the

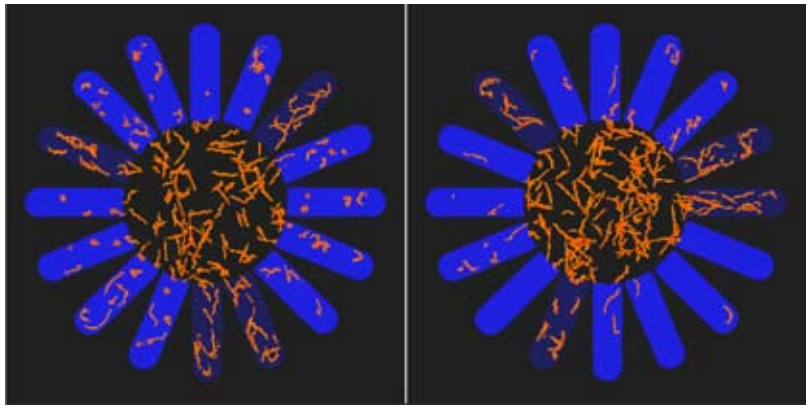

FIGURE 9
Trace images observed at 650 time steps at the best solution #6 (a, left) and 6440 time steps at the best solution #7 (b, right).

average number of *Euglena* cells in one illuminated branch is 4.4 times smaller than that in one non-illuminated branch. This indicates that a smaller γ in *Euglena*-based neurocomputing originates from the reduction in cell number in the illuminated areas rather than the reduction in the swimming speed of the cells in the areas. The reduction in cell number in the illuminated areas is caused by the photophobic reaction of *Euglena* cells at the border of the illumination; *Euglena* cells swimming toward an illuminated area change their swimming direction on encountering the blue light before they are captured in the light.

The transition among the best solutions observed in Fig. 8(a) is triggered by the fluctuation in TMs, as also observed in the simulation [30,31]. However, the origin of the TM fluctuation in real *Euglena*-based neurocomputing is primarily due to the existence of photo-insensitive robust *Euglena* cells, not due to simple statistical fluctuation in TMs in the simulation. Although the number of *Euglena* cells in the illuminated branches is gradually reduced [Fig. 9(b)], some photo-insensitive robust *Euglena* cells swim into the branches eventually, causing status transition in neurocomputing.

The number of *Euglena* cells in the illuminated branches in our *Euglena*-based neurocomputing is determined by four factors: the photosensitivity of *Euglena* cells to change the swimming direction before they are captured in the blue light, the drift capability to escape from the blue light, the robustness to blue light to continue swimming, and the adaptation to the blue light. Photosensitivity and robustness are the personality of individual *Euglena* cells, whereas drift capability and adaptation depend on the temporal evolution of metabolism balance in their bodies [41–43].

The geometry of the micro-aquarium would also affect the performance of *Euglena*-based neurocomputing; when the branch length increases, the probability of the transition among the best solutions observed in Fig. 8(a) will decrease because the number of *Euglena* cells in illuminated branches decreases more slowly for longer branches. In other words, we can control the frequency of the transition among the best solutions by changing the geometry of the micro-aquarium. The geometry of the micro-aquarium in Fig. 1(a) has the same shape (with a reduced size) that was used in amoeba-based computing [28].

On the other hand, the total number of *Euglena* cells in the micro-aquarium does not affect the performance of *Euglena*-based neurocomputing, when the number is not too small (less than approximately 50). Even when approximately 400 cells are used in the aquarium, they swim across each other without collisions, probably because the movement of their flagella avoids collisions by changing swimming depth automatically. Therefore, cell-cell collision effects are negligible in *Euglena*-based neurocomputing even with a large cell density. As in the simulation, the transition among the

best solutions was suppressed when the total cell number is increased because fluctuation in TMs becomes smaller.

3.5 *Euglena* behaviour and interaction

Most essential issues in *Euglena*-based neurocomputing are whether each cell develops/advances its behaviour against photoexposure in the course of the experiments and whether the cells interact each other to realize any collective behaviour.

When a cell is exposed to blue light, the cell is metabolically damaged depending on the exposure duration, and cannot recover its original swimming speed for 20–30 s or longer. This photoexposure history can be considered as a memory effect built in each *Euglena* cells. Cells with slower swimming speeds have a larger chance to draw back on encountering light. In this sense, *Euglena* cells can develop their anti-photoexposure behaviours.

Compared to a slime mould in amoeba-based neurocomputing, in which some aspects of the environment are being communicated within the plasmodium via internal transport or oscillatory behaviour, the cells in *Euglena*-based neurocomputing are primarily independent individuals without explicit communication with each other. However, *Euglena* cells may sense chemicals emitted by other cells. Indeed, we observed that *Euglena* cells tend to avoid entering an area non-illuminated but once irradiated by a strong UV light. We speculate that UV-exposed cells emitted alert-chemicals to the environment, which signals to the other cells not to come close. This observation suggests that *Euglena* cells may take a kind of collective behavior by sensing environmental chemicals.

When *Euglena* cells have a memory effect against photoexposure or when they sense alert chemicals from others, they can avoid entering illuminated branches in *Euglena*-based neurocomputing, leading to the stabilization of the best solutions. On the other hand, when *Euglena* cells sense the concentration of nutrition, they may avoid branches containing a large amount of cells and lacking nutrition, leading to increase in transition frequency among the best solutions. The influences of memory effect and chemical sensing effects are to be elucidated in the future investigations.

3.6 Choice of state variables and functions

In our *Euglena*-based neurocomputing, the TMs of 16 branches in the micro-aquarium in Fig. 1(a) were used as state variables. However, we can use other indices of *Euglena* viability such as TOM or length of swimming traces. When TOM is used as the state variable with the inverted logics for Eq. (3), the performance of *Euglena*-based neurocomputing will be completely different from that described here; the transition among the best

solutions will be promoted by the reduction in *Euglena* cell number in illuminated areas.

We used the sigmoid function in Eq. (2) to normalize the state variable from 0 to 1, with the dynamic auto-adjustment of parameters b and c. The empirical auto-adjustment algorithm in Eqs. (5)–(7) has a large effect on the performance of *Euglena*-based neurocomputing, which must be clarified in further investigations. Furthermore, functions other than the sigmoid function can be used to convert the state variables from 0 to 1, leading to the unexplored behavior of *Euglena*-based neurocomputing.

In this study, the photophobic reactions in *Euglena*-based neurocomputing were evoked by the digital control (On/Off) of the blue light. Because the photophobic reactions of *Euglena* cells depend on the blue light intensity (Fig. 5), we can expect a different transition behavior among the best solutions by using analog feedback (changing blue light intensity continuously) instead of digital feedback.

4 CONCLUSION

We examined *Euglena*-based neurocomputing with the modified Hopfield–Tank algorithm on the basis of the experimentally determined blue light intensity to evoke photophobic reactions of *Euglena* and the empirically derived auto-adjustment of parameters in the feedback algorithm. We verified that the *Euglena*-based neurocomputing for 4-city TSP possesses the fundamental characteristics of (1) attaining one of the best solutions of the problem, and (2) searching for a number of solutions via dynamic transition among the solutions (multi-solution search). Unlike the Monte Carlo simulation previously studied, the essential mechanisms responsible for (1) and (2) in real *Euglena* neurocomputing are the reduction in cell number in illuminated areas and the existence of photo-insensitive robust cells. The choice of state variables, normalization function, and analog feedback are potential to expand the *Euglena*-based neurocomputing performance.

ACKNOWLEDGEMENTS

The authors would like to thank very much Mr. Kengo Suzuki and Ms. Sharbanee Mitra at *Euglena* Co., Ltd., (http://Euglena.jp/) for supplying *Euglena* cells and suggestive information on their nature. They also thank Dr. Masashi Aono for 4-city TSP discussion. They acknowledge financial support for this study by the Ministry of Education, Science, Sports and Culture, Grant-in-Aid for Scientific Research (B), 21360192, 2009-2012. This research was supported partially by the International Research & Development Program of the National Research Foundation of Korea

(NRF) funded by the Ministry of Education, Science and Technology (MEST) of Korea (Grant number: K20901000006-09E0100-00610) and the Seoul R&BD Program (10919).

REFERENCES

[1] J. J. Wolken, E. Shin, *J. Eukaryotic Microbiol.*, **5** (1958) 39. Photomotion in Euglena gracilis I. Photokinesis II. Phototaxis

[2] B. Diehn, *Science*, **181** (1973) 1009. Phototaxis and Sensory Transduction in Euglena

[3] J. J. Wolken, *J. Eukaryotic Microbiol.*, **24** (1977) 518. Euglena: The Photoreceptor System for Phototaxis

[4] M. Ntefidou, M. Iseki, M. Watanabe, M. Lebert, D. P. Häder, *Plant Physiol.*, **133** (2003) 1517. Photoactivated Adenylyl Cyclase Controls Phototaxis in the Flagellate Euglena gracilis

[5] J. Adler, *J. General, Microbiol.*, **74** (1973) 77. Method for Measuring Chemotaxis and Use of the Method to Determine Optimum Conditions for Chemotaxis by Escherichia coli

[6] J. E. Segall, M. D. Manson. H. C. Berg, *Nature*, **296** (1982) 855. Signal processing times in bacterial chemotaxis

[7] R. Zhao, E. J. Collins, R. B. Bourret, R. E. Silversmith, *Nature Structural Biol.*, **9** (2002) 570. Structure and catalytic mechanism of the E. coli chemotaxis phosphatase CheZ

[8] J. S. Parkinson, *J. Bacteriol.*, **185** (2003) 1492. Bacterial Chemotaxis: a New Player in Response Regulator Dephosphorylation

[9] D. Greenfield, A. L. McEvoy, H. Shroff, G. E. Crooks, N. S. Wingreen, E. Betzig, J. Liphardt, *PLoS Biol.*, **7** (2009) 1000137. Self-organization of the Escherichia coli chemotaxis network imaged with super-resolution light microscopy

[10] M. Ntefidou, D.P. Hader, *Photochem. Photobiol. Sci.*, **4** (2005) 732. Photoactivated adenylyl cyclase (PAC) genes in the flagellate Euglena gracilis mutant strains

[11] S. Yoshikawa, T. Suzuki, M. Watanabe, M. Iseki, *Photochem. Photobiol. Sci.*, **4** (2005) 727. Kinetic analysis of the activation of photoactivated adenylyl cyclase (PAC), a blue-light receptor for photomovements of Euglena

[12] *Pili and Flagella: Current Research and Future Trends*, ed. K. Jarrell, Caister Academic Press, Norfolk UK, 2009

[13] L. Barsanti, P. Coltelli, V. Evangelista, V. Passarelli, A. M. Frassanito, N. Vesentini, F. Santoro, P. Gualtieri, *Photochem. Photobiol.*, **85** (2009) 304. In vivo absorption spectra of the two stable states of the Euglena photoreceptor photocycle

[14] B. Diehn, *Biochimica et Biophysica Acta*, **177** (1969) 136. Action spectra of the phototactic responses in Euglena

[15] D. P. Häder, M. Lebert, *Photochem. Photobiol.*, **68** (1998) 260. The photoreceptor for phototaxis in the photosynthetic flagellate Euglena gracilis

[16] E. Kussell, R. Kishony, N. Q. Balaban, S. Leibler, *Genetics*, **169** (2005) 1807. Bacterial Persistence: A Model of Survival in Changing Environments

[17] D. Dubnau, R. Losick, *Mol. Microbiol.*, **61** (2006) 564. Bistability in bacteria

[18] S. V. Avery, *Nature Rev. Microbiol.*, **4** (2006) 577. Microbial cell individuality and the underlying sources of heterogeneity

[19] T. Nakagaki, H. Yamada, A. Toth, *Nature*, **407** (2000) 470. Maze-Solving by an Amoeboid Organism

[20] M. Aono, Y.-P. Gunji, *Biosystems*, **71** (2003) 257. Beyond Input-Output Computings: Error-Driven Emergence with Parallel No-Distributed Slime Mold Computer

[21] S. Tsuda, M. Aono, Y.-P. Gunji, Y.-P., *Biosystems*, **73** (2004) 45. Robust and emergent Physarum logical-computing

[22] R. Kobayashi, A. Tero, T. Nakagaki, *J. Math. Biol.*, **53** (2006) 273. Mathematical model for rhythmic proto-plasmic movement in the true slime mold

[23] M. Aono, M. Hara, K. Aihara, *Commum.ACM*, **50** (2007) 69. Amoeba-based Neurocomputing with Chaotic Dynamics

[24] S. Tsuda, K. Zauner, Y. Gunji, *Biosystems*, **87** (2007) 215. Robot control with biological cells

[25] A. Tero, R. Kobayashi, T. Nakagaki, *J. Theoret. Biol.*, **244** (2007) 553. A mathematical model for adaptive transport network in path finding by true slime mold

[26] M. Aono, M. Hara, *Biosystems*, **91** (2008) 83. Spontaneous deadlock breaking on Amoeba-based neurocomputer

[27] A. Adamatzky, J. Jones, *J. Bionic Eng.*, **5** (2008) 348. Towards physarum robots: conputing and manipulating on water surface

[28] M. Aono, Y. Hirata, M. Hara, K. Aihara, *New Generation Computing*, **27** (2009) 129. Amoeba-based Chaotic Neurocomputing: Combinatorial Optimization by Coupled Biological Oscillators

[29] A. Adamatzky, *Parallel Processing Lett.*, **19** (2009) 105. Developing proximity graphs by physarum polycephalum: Does the plasmodium follow toussaint hierarchy?

[30] K. Ozasa, M. Aono, M. Maeda, M. Hara, *Lecture Notes in Computer Science*, **5715** (2009) 209. Simulation of Neurocomputing Based on Photophobic Reactions of Euglena - Toward Microbe-Based Neural Network Computing -

[31] K. Ozasa, M. Aono, M. Maeda, M. Hara, *Biosystems*, **100** (2010) 101. Simulation of neurocomputing based on the photophobic reactions of Euglena

[32] *The Biology of Euglena*. Vol IIn: ed. D. E. Buetow, Academic Press, New York, 1968.

[33] *The Biology of Euglena*. Vol IIIn: ed. D. E. Buetow, Academic Press, New York, 1968.

[34] *The Biology of Euglena*. Vol IIIIn: ed. D. E. Buetow, Academic Press, New York, 1982.

[35] M. Cramer, J. Myers, *Arch. Mikrobiol.*, **17** (1952) 384. Growth and photosyntlhetic characteristics of Euglena gracilis

[36] K. Ozasa, J. Lee, S. Song, M. Hara, M. Maeda, *Lab. Chip*, **11** (2011) 1933. Two-dimensional optical feedback control of Euglena confined in closed-type microfluidic channels

[37] A. Baldassarrel, M. D. Lucial, P. Nesi, F. Rossil, *Real Time Imaging*, **7** (2001) 145. A Vision-Based Particle Tracking Velocimetry

[38] C. Liu, L. Tao, *J. Coastal Res.*, **SI50** (2007) 415. Two-Dimensional Digital Particle Tracking Velocimetry Algorithm Based on the Image of Particle Trace

[39] J. J. Hopfield, D. W. Tank, *Science*, **233** (1986) 625. Computing with Neural Circuits: A model

[40] *Neural computing: theory and practice*, P. D. Wasserman, Van Nostrand Reinhold, New York, U.S.A. (1989)

[41] A. Novick, M. Weiner, *Proc. Natl. Acad. Sci. USA*, **43** (1957) 553. Enzyme induction as all-or-none phenomenon

[42] J. Casadesus, D. A. Richard, *Bio Essays*, **24** (2002) 512. Memory in bacteria and phage

[43] M. Inoue, K. Kaneko, *Phys. Rev. E*, **77** (2008) 041916. Conditions for self-consistent aggregation by chemotactic particles